Detection of Cardiac Occlusions Using Viscoelastic Wave Propagation

H.T. Banks and J. R. Samuels, Jr.

Center for Research in Scientific Computation
North Carolina State University
Raleigh, NC 27695-8212

December 12, 2008

Abstract

We consider the problem of detecting cardiac artery occlusions using stenosis driven viscoelastic (VE) waves propagated through biotissue to body surface sensors. We investigate possible statistical model formulations (ordinary least squares (OLS), generalized least squares (GLS)) and post analysis techniques (residual plots) to ascertain uncertainty in estimates as well as validity of the statistical models as part of a methodology for stenosis detection using viscoelastic waves.

Key Words: Inverse problems, viscoelastic models, wave propagation in biotissue, statistical models.

AMS Subject Classifications: 34A55, 35R30, 74J25, 62J02, 93A30.

1 Introduction

Coronary artery disease (CAD) is the leading cause of death in many parts of the developed world. The disease is caused by a gradual accumulation of atheromatous plaques (e.g. cholesterol, fatty acids, calcium and fibrous connective tissue) along the wall of the vessel [1]. Although the symptoms of CAD are pronounced in the later stages of the affliction, it is very difficult to diagnosis the disease before the first onset of symptoms, typically a sudden heart attack [22].

Current detection techniques include angiograms and CT scans. Angiograms are an invasive technique, which typically requires entering the vessel through the femoral artery or the jugular vein - a process many may wish to avoid. On the other hand, CT scans generate a three-dimensional image of an object by taking multiple two-dimensional X-Rays while rotating around an axis and expose a patient to sufficient radiation. In another approach, engineers have developed sensors that can detect the acceleration of acoustic waves [2]. The underlying approach is rather simple: blockages in the artery create turbulence in the blood flow, which then generates an acoustic wave with a normal and shear component (Figure 1). The acoustic wave propagates through the chest cavity until it reaches the chest wall, where a series of sensors would detect the acceleration of the components of the wave. The data from the sensors might then be used to quickly determine the location of the blockages, if any, in the artery. Unlike the other detection techniques discussed above, the process would be inexpensive and non-invasive.

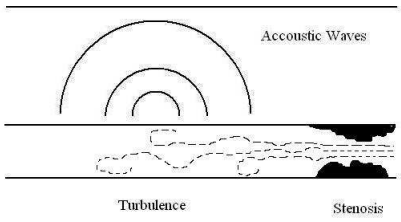

Figure 1: Depiction of interaction between arterial blockage and acoustic wave.

For such a technology to be feasible, a mathematical model that describes the propagation of the acoustic wave from the stenosis to the chest wall would be necessary. One, two and three dimensional models have been developed [2, 21, 23] as investigators continued efforts on scientific issues, especially the feasibility of detecting and locating the stenosis. In [11, 21], the authors identified lingering issues with inverse problems and reliability of estimates of parameters even in the two-dimensional models. Here we report further efforts and results related to the efficacy of the inverse problem involving a two-dimensional version of the model and simulated noisy data.

In particular we consider VE models for stenosis driven wave simulations and demonstrate that the corresponding inverse problems are computationally tractable even though they involve computationally challenging forward problems. Specifically, we show that one can implement the inverse problem for estimation of both geometric and material parameters in the VE wave propagation models. We consider how one ascertains reliability of estimates and show by example one approach to the computation of standard errors and confidence intervals. As we detail below, there exist asymp-

totic theories for error analysis – whether for absolute error (OLS) or for relative error (GLS) in the data, but one does not know *a priori* what type of error model to assume. As we demonstrate by computational examples, one must use the correct statistical model for the standard errors computed to be meaningful (one could err because one could assume incorrect error ϵ or incorrect model response $f(t, \theta_0)$). As we show, one cannot make judgements regarding correct statistical model assumptions by simply comparing standard errors. We argue that residual plot analysis offers one approach to investigating correctness of statistical model assumption. Finally, our presentation here demonstrates the effectiveness of a mathematical and statistical inverse problem methodology in identifying both material and geometric occlusion parameters in a 2D model for arterial stenosis detection.

2 Model Formulation

In [11, 21] the authors developed a two dimensional internal strain variable (ISV) model that describes how VE waves that are caused by arterial blockages propagate through biotissue. For the two-dimensional geometry, the authors assumed that the sensors would be located on the chest wall $r = R,\ \phi = \phi_i,\ i = 1, \ldots, m$ and would detect the acceleration of VE waves from within the chest cavity (see Figure 2). The acceleration data would then be compared to the model to determine if a stenosis is located in the artery. Although the two-dimensional model contains a number of parameters (e.g., the relaxation parameters ν_{λ_k} and ν_{μ_k}), the two of particular interest represent the location of the occlusion along the inner wall of a circular geometry (see Figure 2).

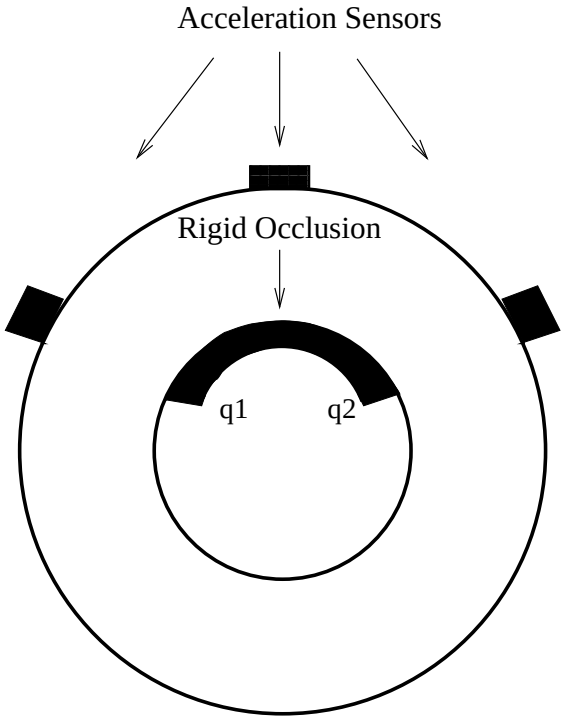

Figure 2: Geometry with occlusion along the inner radius $r = r_1$.

The model in [11, 21, 23] is sophisticated; however, one should not be under the illusion that it (or any model) perfectly describes the situation at hand. It is not difficult to imagine that noise generated from measurement error or biological influences from within the chest cavity might corrupt the data. Thus one needs to investigate how random noise might impact the model. Ideally, we would like to begin this investigation by comparing the OLS estimates $\hat{\theta}_{\text{OLS}}$ and GLS estimates $\hat{\theta}_{\text{GLS}}$ for the geometric parameters $\vec{\theta} = (q_1, q_2)^T$ to each other, but the discontinuous occlusion geometry (see Figure 2) prevents a straightforward optimization [21]. Unless we alter the geometry of the occlusion we will be unable to compare $\hat{\theta}_{\text{OLS}}$ to $\hat{\theta}_{\text{GLS}}$ for $\vec{\theta} = (q_1, q_2)^T$.

There are, however, parameters embedded continuously in the model, which will allow us to calculate $\hat{\theta}_{\text{GLS}}$. The model dynamics as developed in [11, 21, 23] are given in polar co-ordinates (r, ϕ) by

$$\rho \frac{\partial^2 u_1}{\partial t^2} = \sum_{k=1}^{K} \left\{ \frac{\partial}{\partial r}\left(\epsilon_{\lambda_k} + \epsilon_{\mu_k}^{11}\right) + \frac{1}{r}\frac{\partial}{\partial \phi}\left(\epsilon_{\mu_k}^{21}\right) + \frac{1}{r}\left(\epsilon_{\mu_k}^{11} - \epsilon_{\mu_k}^{22}\right) \right\} \tag{1}$$

$$\rho \frac{\partial^2 u_2}{\partial t^2} = \sum_{k=1}^{K} \left\{ \frac{\partial}{\partial r}\left(\epsilon_{\mu_k}^{12}\right) + \frac{1}{r}\frac{\partial}{\partial \phi}\left(\epsilon_{\lambda_k} + \epsilon_{\mu_k}^{22}\right) + \frac{1}{r}\left(\epsilon_{\mu_k}^{12} + \epsilon_{\mu_k}^{21}\right) \right\} \tag{2}$$

$$\frac{\partial \epsilon_{\lambda_k}}{\partial t} = -\nu_{\lambda_k}\epsilon_{\lambda_k} + C_{\lambda_k}\frac{\partial}{\partial t}\left(S_{11}^{(\text{e})} + S_{22}^{(\text{e})}\right) \tag{3}$$

$$\frac{\partial \epsilon_{\mu_k}^{11}}{\partial t} = -\nu_{\mu_k}\epsilon_{\mu_k}^{11} + C_{\mu_k}\frac{\partial}{\partial t}\left(S_{11}^{(\text{e})}\right) \tag{4}$$

$$\frac{\partial \epsilon_{\mu_k}^{12}}{\partial t} = -\nu_{\mu_k}\epsilon_{\mu_k}^{12} + C_{\mu_k}\frac{\partial}{\partial t}\left(S_{12}^{(\text{e})}\right) \tag{5}$$

$$\frac{\partial \epsilon_{\mu_k}^{22}}{\partial t} = -\nu_{\mu_k}\epsilon_{\mu_k}^{22} + C_{\mu_k}\frac{\partial}{\partial t}\left(S_{22}^{(\text{e})}\right), \quad k = 1, \ldots, K. \tag{6}$$

The relevant terms in the model are the radial ($u_1 = u_r$) and tangential ($u_2 = u_\phi$) displacements, respectively, the "elastic" stress tensor $\{S_{ij}^{(\text{e})}\}$ [18, 20] and the *internal strain variables* (ISV) ϵ_{λ_k} and $\epsilon_{\mu_k}^{kl}$. The elastic stress tensor elements are computed using strain energy functions (SEFs) as explained in Chapter 4 of [23] and are functions of the Green's strains $E_{11} = \frac{\partial u_1}{\partial r}$, $E_{22} = \frac{1}{r}(u_1 + \frac{\partial u_2}{\partial \phi})$, and $E_{12} = E_{21} = \frac{1}{r}\frac{\partial u_1}{\partial \phi} + \frac{\partial u_2}{\partial r} - \frac{u_2}{r}$. The parameters C_{λ_k} and C_{μ_k}, $k = 1, \ldots, K$, are amplitude coefficients for input to the internal strain variables used in approximating the reduced relaxation parameter G in Fung's quasi-linear viscoelastic (VE) model [17]. The parameters q_1 and q_2 arise in the inner radius boundary conditions (see Figure 2). It's obvious that the model depends continuously on the parameters C_{λ_k} and C_{μ_k}; hence those parameters are better candidates for estimation via an inverse problem formulation than are q_1 and q_2. The remainder of the parameters (ν_{λ_k} and ν_{μ_k}) will be taken as fixed in the estimation procedures described below even though they are also readily estimated.

To derive equations (1)-(6), we first combine the equation of continuity with momentum balance equations in linear elasticity theory [18, 20] to obtain

$$\rho \frac{\partial^2 u_1}{\partial t^2} = \frac{\partial S_{11}}{\partial r} + \frac{1}{r}\left(S_{11} - S_{22}\right) + \frac{1}{r}\frac{\partial S_{21}}{\partial \phi} \tag{7}$$

$$\rho \frac{\partial^2 u_2}{\partial t^2} = \frac{1}{r}\left(S_{12} + S_{21}\right) + \frac{\partial S_{12}}{\partial r} + \frac{1}{r}\frac{\partial S_{22}}{\partial \phi}, \tag{8}$$

where $\{S_{ij}\}$ is the internal stress tensor. Next we consider Fung's Quasilinear Viscoelasticity (QLV) constitutive equation theory [17] for the internal stresses in biological tissue given by

$$S_{ij}(t) = \sum_{kl} \int_{-\infty}^{t} G_{ijkl}(t-\tau) \frac{\partial S_{kl}^{(e)}(\bar{E}(\tau))}{\partial \tau} d\tau, \tag{9}$$

where $\bar{E}$ is the Green's strain tensor, G_{ijkl} is the Fung reduced ($G_{ijkl}(0) = 0$) relaxation or kernel function. The Green's strain tensor $\bar{E}(\tau) = \{E_{ij}(\tau)\}$ is symmetric and is commonly used when materials undergo small deformations, while the elastic stress tensor $S^{(e)} = \{S_{ij}^{(e)}\}$ describes the material's response to a sudden application of a step function [17].

In [2] the authors substantially decreased computational time (a highly desirable goal in inverse problem applications) by approximating Fung's one dimensional quasilinear VE model

$$\sigma(t) = \int_{-\infty}^{t} G(t-\tau) \frac{\partial S^{(e)}(\bar{E}(\tau))}{\partial \tau} d\tau \tag{10}$$

using internal variables $\tilde{\epsilon}_k$ (in $\sigma(t) = \sum_{k=1}^{K} \tilde{\epsilon}_k(t)$). To employ the internal variable approach the authors assumed that the material properties can be well approximated by those of a material with a finite number of relaxation times (instead of a continuous spectrum of relaxation times as Fung proposed). The assumption is equivalent to approximating G in (10) by a finite sum of exponential functions:

$$G(t) = \sum_{k=1}^{K} C_k e^{-t/\tau_k}.$$

The main advantage to using internal variables in (9) with the equations of motion in the one-dimensional case is that the dynamical system can be integrated much more quickly without a significant loss of accuracy [2].

Although it might be obvious why such an approximation would be computationally beneficial, it is not as obvious what the K internal variables $\{\tilde{\epsilon}_k\}$ physically represent. We approximate Fung's kernel resulting in a family of *internal variable strains*. The underlying assumption involves treating the molecules within the biological tissue as elastic on a microscopic scale. Thus, the stress response σ_{ij} of a particular molecule within the material (on a microscopic scale) takes the form

$$\sigma_{ij} = \sum_{kl} G_{ijkl} e_{kl}, \tag{11}$$

where e_{kl} is the strain applied to the molecule of interest. If $G_{ijkl} = G_{jikl}$ and $G_{ijkl} = G_{ijlk}$ then the tensor G_{ijkl} can be written [18]

$$G_{ijkl}(t) = \lambda(t)\delta_{ij}\delta_{kl} + \mu(t)\left(\delta_{ik}\delta_{jl} + \delta_{il}\delta_{jk}\right), \tag{12}$$

where λ and μ are generalized Lamé parameters. The constitutive law then takes the

form

$$S_{ij}(t) = \sum_{kl} \int_{-\infty}^{t} \{\lambda(t-\tau)\delta_{ij}\delta_{kl} + \mu(t-\tau)(\delta_{ik}\delta_{jl} + \delta_{il}\delta_{jk})\} \frac{\partial S_{kl}^{(e)}(\bar{E}(\tau))}{\partial \tau} d\tau \tag{13}$$

$$= \int_{-\infty}^{t} \left\{ \lambda(t-\tau) \frac{\partial}{\partial \tau} \left(S_{11}^{(e)}(\bar{E}(\tau)) + S_{22}^{(e)}(\bar{E}(\tau)) \right) \delta_{ij} + 2\mu(t-\tau) \frac{\partial S_{ij}^{(e)}(\bar{E}(\tau))}{\partial \tau} \right\} d\tau. \tag{14}$$

Depending on the form assumed for λ and μ, the above formulation assumes that all molecules react in the same manner at the microscopic level. Previous work in one dimension [12] suggests that multiple *internal variables* might be used to represent various subclasses of molecules in a particular material. For instance, if a tissue sample is comprised primarily of three different (elastic) types of molecules, then there would be $K = 3$ internal variables each identified by a particular relaxation time $\tau_k = \frac{1}{\nu_k}$. As shown in [12], a finite number of such subclasses of molecules can often be successfully used as a good approximation to a continuum of subclasses of molecules (i.e., the Fung approach): an identical approach was employed in the two dimensional case [21] with success.

The same approach can be utilized in higher dimensions. To do so, we will approximate the parameters $\lambda(t)$ and $\mu(t)$ in (12) by series of exponentials, such that

$$\lambda(t) \approx \sum_{k} C_{\lambda_k} e^{-\nu_{\lambda_k} t} \quad \mu(t) \approx \sum_{k} C_{\mu_k} e^{-\nu_{\mu_k} t}. \tag{15}$$

If these exponential parameters are used in (14) then the stress tensor S_{ij} can be approximated as

$$S_{ij}(t) \approx \sum_{k} \left\{ \epsilon_{\lambda_k}(t)\delta_{ij} + \epsilon_{\mu_k}^{ij}(t) \right\}, \tag{16}$$

where

$$\epsilon_{\lambda_k}(t) = \int_{-\infty}^{t} \left[C_{\lambda_k} e^{-\nu_{\lambda_k}(t-\tau)} \frac{\partial}{\partial \tau} \left(S_{11}^{(e)}(\bar{E}(\tau)) + S_{22}^{(e)}(\bar{E}(\tau)) \right) \right] d\tau \tag{17}$$

$$\epsilon_{\mu_k}^{ij}(t) = \int_{-\infty}^{t} \left[2C_{\mu_k} e^{-\nu_{\mu_k}(t-\tau)} \frac{\partial S_{ij}^{(e)}(\bar{E}(\tau))}{\partial \tau} \right] d\tau \tag{18}$$

are *internal variables* with $\epsilon_{\lambda_k}(0) = 0$ and $\epsilon_{\mu_k}^{ij}(0) = 0$. Note that the form of equations (17) and (18) can be written (using the variation of parameters formula) as solutions to linear differential equations

$$\frac{\partial \epsilon_{\lambda_k}}{\partial t} = -\nu_{\lambda_k}\epsilon_{\lambda_k} + C_{\lambda_k} \frac{\partial}{\partial t} \left(S_{11}^{(e)}(\bar{E}(t)) + S_{22}^{(e)}(\bar{E}(t)) \right), \quad \epsilon_{\lambda_k}(0) = 0 \tag{19}$$

$$\frac{\partial \epsilon_{\mu_k}^{ij}}{\partial t} = -\nu_{\mu_k}\epsilon_{\mu_k}^{ij} + 2C_{\mu_k} \frac{\partial}{\partial t}(S_{ij}^{(e)}(\bar{E}(t))), \quad \epsilon_{\mu_k}^{ij}(0) = 0, \tag{20}$$

which, when combined with (7), (8) and (16), yields (1)–(6).

We remark that models employing (15) and (16) are special cases of models with a continuum of relaxation times $\tau = 1/\nu$ as formulated in [12, 13]. Specifically, we define generalized constitutive laws embodying Lamé parameters

$$\lambda(t) = \int_{\Lambda} e^{-\nu_\lambda t} d\mathcal{P}_1(\lambda), \quad \mu(t) = \int_{\mathcal{M}} e^{-\nu_\mu t} d\mathcal{P}_2(\mu) \tag{21}$$

with probability measures $\mathcal{P}_1(\lambda)$, $\mathcal{P}_2(\mu)$, defined respectively on the bounded continuum sets Λ, $\mathcal{M}$, along with the corresponding continuum version of (16) given by

$$S_{ij}(t) = \delta_{ij} \int_{\Lambda} \{\epsilon_\lambda(t) d\mathcal{P}_1(\lambda)\} + \int_{\mathcal{M}} \left\{\epsilon_\mu^{ij}(t) d\mathcal{P}_2(\mu)\right\} \tag{22}$$

where

$$\epsilon_\lambda(t) = \int_{-\infty}^{t} \left[C_\lambda e^{-\nu_\lambda(t-\tau)} \frac{\partial}{\partial \tau} \left(S_{11}^{(e)}(\bar{E}(\tau)) + S_{22}^{(e)}(\bar{E}(\tau)) \right) \right] d\tau \tag{23}$$

$$\epsilon_\mu^{ij}(t) = \int_{-\infty}^{t} \left[2C_\mu e^{-\nu_\mu(t-\tau)} \frac{\partial S_{ij}^{(e)}(\bar{E}(\tau))}{\partial \tau} \right] d\tau. \tag{24}$$

These constitutive laws have a continuum of relaxation parameters and moreover, it is shown in [3] that the set of finite rational convex combinations of Dirac measures Δ_a (with atom at a) of the form

$$\mathcal{P}_1(\lambda) = \sum_k a_k \Delta_{\lambda_k}(\lambda), \quad \mathcal{P}_2(\mu) = \sum_k b_k \Delta_{\mu_k}(\mu) \tag{25}$$

are dense in the Prohorov metric [4] in the set of all probability measures on Λ and $\mathcal{M}$, respectively. This can be used to argue that (15)-(18) do indeed provide finite spectrum constitutive law approximations to the continuum spectrum constitutive laws.

As noted above, Fung's kernel as developed in [17] embodies a continuous spectrum of relaxation times in the constitutive law (9). With his kernel Fung was able to significantly enhance the mathematical description of the relationship between stress and strain in biological tissue. Unfortunately, if the constitutive law (9) with Fung's reduced relaxation function is used in a dynamical system (such as (7)–(8)), the system is not computationally tractable for use in inverse problems (this is also true for our continuum relaxation spectrum model defined using (21)). One reason for this is that Fung's kernel is formulated with a double integral and so if, for example, a finite difference scheme is used to integrate the equations of motion with the kernel, then at every step the scheme must integrate multiple double integrals - a very time consuming task. To remedy this situation, we approximated Fung's constitutive law (or actually the alternative constitutive law defined via (21)) using a finite number of internal variables. These internal variables lead to a form of the equations of motion and dynamical system that is not only computationally tractable but also whose *solutions* closely approximate *solutions* of systems utilizing Fung's kernel or the generalized law involving (21) (at least in the one-dimensional setting [2]). We use this model to demonstrate inverse problem concepts and capabilities with simulated noisy acceleration data.

3 Inverse Problems

In inverse problems involving the internal strain variable models formulated in the previous section, there are two distinct types of problems that one might consider: ones involving estimation of *material* parameters such as ν_{λ_k}, ν_{μ_k}, C_{λ_k}, and C_{μ_k}, and ones involving estimation of *geometric* parameters such as the occlusion parameters q_1 and q_2. Moreover, in such problems there are two primary types of noisy data most frequently encountered: measurements with absolute (and constant variance) error and measurements with relative error (and hence nonconstant model-dependent variance).

To treat such data one usually employs either ordinary least squares (OLS) or generalized least squares (GLS) formulations corresponding to the statistical model assumed. We recall [5] that in any inverse problem formulation one requires both a *mathematical model* (such as (1)-(6)) and a *statistical model* as described in [5]). In this paper we will investigate two popular statistical models and the corresponding estimators, the ordinary least squares (OLS) estimators $\theta_{\rm OLS}$ defined by

$$\theta_{\rm OLS} = \arg\min_{\vec{\theta}\in\Theta} \sum_{j=1}^{n} \left(\vec{Y}_j - \vec{f}\big(t_j,\vec{\theta}\big)\right)^T V_0^{-1} \left(\vec{Y}_j - \vec{f}\big(t_j,\vec{\theta}\big)\right), \tag{26}$$

and the generalized least squares (GLS) estimators $\theta_{\rm GLS}$ defined here as the limit as $k\to\infty$ of the sequence of solutions to minimizing problems

$$\theta_{\rm GLS}^{(k+1)} = \arg\min_{\vec{\theta}\in\Theta} \sum_{j=1}^{n} f^{-2}(t_j,\theta_{\rm GLS}^{(k)}) \left(Y_j - f\big(t_j,\vec{\theta}\big)\right)^2, \tag{27}$$

to estimate various parameters in an ISV model of the form (1)-(6) for waves in VE tissue. (The usual definition involves normal equations as discussed in [5, 15].) The weighting terms V_0 and $w_j^{(k)} = f^{-2}(t_j,\theta_{\rm GLS}^{(k)})$ are related to the assumed statistical model. For instance, if the data arises from measurements described by a *constant* variance (CV) statistical model (absolute error)

$$\vec{Y}_j = \vec{f}(t_j,\vec{\theta}_0) + \vec{\epsilon}_j \tag{28}$$

where $\vec{f}\in R^m$, then

$$V_0 = {\rm var}(\vec{\epsilon}_j) = {\rm diag}(\sigma_{0,1}^2,\ldots,\sigma_{0,m}^2) \tag{29}$$

for $j=1,\ldots,n$. In this case the OLS formulation is appropriate. However, if the data is generated from the *nonconstant* variance (NCV) statistical model such as one with relative measurement error

$$Y_j = f(t_j,\vec{\theta}_0)\,(1+\epsilon_j)\,, \tag{30}$$

then ${\rm var}(Y_j) = \sigma_0^2 f^2(t_j,\vec{\theta}_0) = \sigma_0^2 (w_j(t_j,\vec{\theta}_0))^{-1}$ so that a GLS formulation is most appropriate. (Here f is any one of the scalar sensor accelerations $\frac{\partial^2 u_1}{\partial t^2}$.) We can obtain an estimate $\hat{\theta}_{\rm OLS}$ (or $\hat{\theta}_{\rm GLS}$) of the random variable $\theta_{\rm OLS}$ (or $\theta_{\rm GLS}$) if there exists a realization, say $\{\vec{y}_j\}_{j=1}^n$ (or $\{y_j\}_{j=1}^n$), of the random variable $\{\vec{Y}_j\}_{j=1}^n$ (or $\{Y_j\}_{j=1}^n$). Of course, one rarely *knows in advance* the form of the error structure present in the data. Thus we shall investigate both OLS and GLS formulations to demonstrate their

feasibility if the correct statistical model for the data is chosen. Moreover, we shall present and illustrate post inverse problem methodology for ascertaining whether one has made a reasonable choice for the statistical model. From our discussions, it will be clear that the mathematical model is dictated by the underlying dynamics in a problem and the statistical model should be determined by the measurement process that produces the data.

Because there are lingering issues with the inverse problems for the two-dimensional ISV model, we will address the inverse problem in this setting. We note that the model solutions are smooth in the material parameters ν_{λ_k}, C_{λ_k}, etc., while they are not differentiable with respect to the geometric parameters such as $q_1,\ q_2$, when formulated as depicted in Figure 2. Therefore, we will first investigate results from the OLS and GLS methods and the corresponding standard errors from the more well-behaved material parameters (throughout we choose $K = 2$ internal variables in our mathematical models)

$$\vec{\theta} = \begin{pmatrix} C_{\lambda_1} \\ C_{\lambda_2} \\ C_{\mu_1} \\ C_{\mu_2} \end{pmatrix}.$$

To do so the following procedure will be followed:

1. Because we wish to demonstrate the methodology using data with known statistical properties, we first solve (1)-(6) for the compression wave acceleration model response $f_i(t, \vec{\theta}) = \frac{\partial^2 u_1}{\partial t^2}(t, R, \phi_i, \vec{\theta})$ at the chest wall boundary $r = R$ and some sensor location (R, ϕ_i) (we assume there are at most m sensors located at (R, ϕ_i)) with known $\vec{\theta} = \vec{\theta}_0$ defined by

$$\vec{\theta}_0 = \begin{pmatrix} C^0_{\lambda_1} \\ C^0_{\lambda_2} \\ C^0_{\mu_1} \\ C^0_{\mu_2} \end{pmatrix} = \begin{pmatrix} 1187.43236 \\ 1432.64603 \\ 386.639704 \\ 3456.74921 \end{pmatrix}.$$

   (We remark that we could have equally well used shear wave acceleration $f_i(t, \vec{\theta}) = \frac{\partial^2 u_2}{\partial t^2}(t, R, \phi_i, \vec{\theta})$ in our investigations throughout.)

2. Then varying levels of normally distributed error (measurement noise) will be added to these solutions in two ways: with constant variance (CV) and nonconstant variance (NCV). That is, we construct noisy data in the constant variance case by

$$\vec{Y}_j = \vec{f}(t_j, \vec{\theta}_0) + \frac{\alpha}{100}\vec{\epsilon}_j,$$

   with $\vec{\epsilon}_j \sim N(0, V_0)$ and in the nonconstant variance case by

$$Y_j = f(t_j, \vec{\theta}_0)\left(1 + \frac{\alpha}{100}\epsilon_j\right),$$

   where $\epsilon_j \sim \mathcal{N}(0, \sigma_0^2)$ and f is the acceleration at a given sensor. The parameter α allows us to adjust the level of noise introduced in the statistical models.

3. Once noise is added to the data, the noisy data is used to obtain an estimate $\hat{\theta}$ using a numerical implementation of the OLS and GLS formulations for $\alpha = 0, 1, \ldots, 10$.

Therefore, four cases will be considered: the OLS estimate obtained using data generated with constant variance (the correct procedure for the data), the OLS estimate obtained using data generated with nonconstant variance (an incorrect procedure for the data), the GLS estimate obtained using data generated with constant variance (again an incorrect procedure for the data) and the GLS estimate obtained using data generated with nonconstant variance (the correct procedure for the data).

Initially, constant variance was added to the *scalar* model $f_i(t_j, \vec{\theta}_0) = \frac{\partial^2 u_1}{\partial t^2}(t, R, \phi_i, \vec{\theta})$ at the sensor location (R, ϕ_i)

$$Y_j^i = f_i(t_j, \vec{\theta}_0) + \frac{\alpha}{100}\epsilon_j, \tag{31}$$

where $\text{var}(\epsilon_j) = \sigma_0^2$ for $\alpha = 0, \ldots, 10$. However, data from some sensors were swamped by the level of noise introduced. This situation arose from the fact that different sensors had varying scales of acceleration data (see Figure 3). The noise was generated in Figure 3 by setting $\alpha = 3$ and $\epsilon_j \sim \mathcal{N}(0, 1)$. It is obvious that the 1^{st} sensor's reading has not been significantly affected by the noise, but the 5^{th} sensor's data's scale has been totally corrupted.

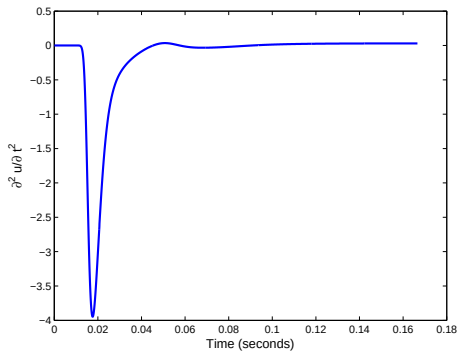

Acceleration Data for the 1^{st} sensor

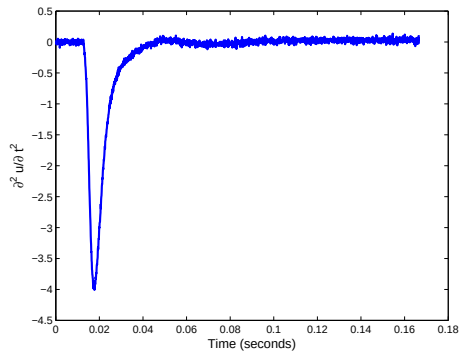

Acceleration Data for the 1^{st} sensor with $\alpha = 3$

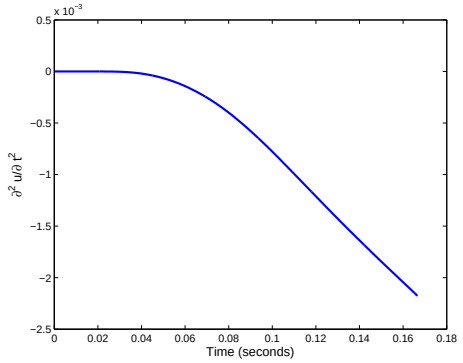

Acceleration Data for the 5^{th} sensor

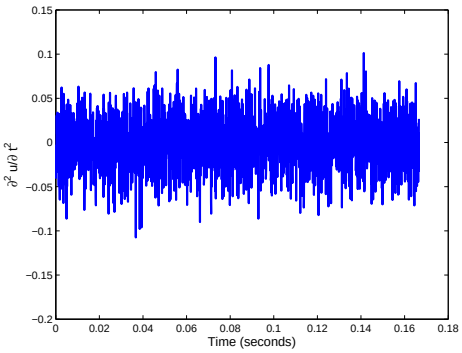

Acceleration Data for the 5^{th} sensor with $\alpha = 3$

Figure 3: Comparison of the scale between the readings of two sensors.

So, instead of implementing a scalar model in the constant variance regime, we will treat the observations in the constant variance case by

$$\vec{Y}_j = \vec{f}(t_j, \vec{\theta}_0) + \frac{\alpha}{100}\vec{\epsilon}_j, \tag{32}$$

where $\text{var}(\vec{\epsilon}_j) = V_0 = \text{diag}(\sigma_{0,1}^2, \ldots, \sigma_{0,m}^2)$ and the i^{th} element of the vector $\vec{Y}_j$ represents the acceleration at the i^{th} sensor on the chest wall. In this regime we can add sensor-specific constant variance error to each element in the array $\vec{f}(t_j, \vec{\theta}_0)$, and thus avoid totally corrupting a given sensor's data. Because nonconstant variance depends upon the model (and hence it's scale) adding nonconstant variance will not swamp any sensors readings. In other words, for nonconstant variance data, we use a simple scalar error ϵ_j to formulate the model and data at each sensor location (R, ϕ_i) as

$$Y_j^i = f_i(t_j, \vec{\theta}_0)\left(1 + \frac{\alpha}{100}\epsilon_j\right),$$

where $f_i(t, \vec{\theta}) = \frac{\partial^2 u_1}{\partial t^2}(t, R, \phi_i, \vec{\theta})$.

3.1 Asymptotic Theories for Error Analysis

To followe the procedure outlined in [23], optimized estimates $\hat{\theta}_{\text{opt}}$ and the corresponding variances for each case were obtained and standard errors computed. The standard errors are computed using the variance of an estimate's asymptotic distribution. The *asymptotic distribution* (as sample size $n \to \infty$) for both methods is a normal ($\mathcal{N}$) distribution and the form of the variance, and hence the standard error, depends upon the error generating term in the statistical model [5, 15, 16, 24]. If the statistical model has constant variance (CV) as in

$$\vec{Y}_j = \vec{f}(t_j, \vec{\theta}_0) + \vec{\epsilon}_j \qquad \text{Var}(\vec{Y}_j) = V_0,$$

and the OLS method is used to estimate $\vec{\theta}_0$, then under a number assumptions [5, 24] on the model and the measurement process, the asymptotic distribution of the estimator θ_{OLS} is given by (see [5] for a detailed discussion)

$$\theta_{\text{OLS}} \sim \mathcal{N}(\vec{\theta}_0, \Sigma_0^n), \tag{33}$$

where

$$\Sigma_0^n \quad = \quad \left(\sum_{j=1}^{n} D_j^T(\vec{\theta}_0) V_0^{-1} D_j(\vec{\theta}_0)\right)^{-1}, \tag{34}$$

and the $m \times p$ matrix $D_j(\vec{\theta}) = D_j^n(\vec{\theta})$ is given by

$$\begin{pmatrix} \frac{\partial f_1(t_j,\vec{\theta})}{\partial \theta_1} & \frac{\partial f_1(t_j,\vec{\theta})}{\partial \theta_2} & \cdots & \frac{\partial f_1(t_j,\vec{\theta})}{\partial \theta_p} \\ \vdots & \vdots & & \vdots \\ \frac{\partial f_m(t_j,\vec{\theta})}{\partial \theta_1} & \frac{\partial f_m(t_j,\vec{\theta})}{\partial \theta_2} & \cdots & \frac{\partial f_m(t_j,\vec{\theta})}{\partial \theta_p} \end{pmatrix}.$$

Because the true value of the parameters $\vec{\theta}_0$ and V_0 are unknown, their estimates $\hat{\theta}$ and $\hat{V}$ are used to approximate the asymptotic properties of the least squares estimator θ_{OLS}:

$$\theta_{\text{OLS}} \sim \mathcal{N}_p(\vec{\theta}_0, \Sigma_0^n) \approx \mathcal{N}_p(\hat{\theta}, \hat{\Sigma}^n), \tag{35}$$

where

$$\Sigma_0^n \approx \hat{\Sigma}^n = \left(\sum_{j=1}^{n} D_j^T(\hat{\theta}) \hat{V}^{-1} D_j(\hat{\theta}) \right)^{-1}. \tag{36}$$

The standard errors of the parameters can then be calculated by taking the square root of the diagonal elements of (36).

On the other hand, if the statistical model has nonconstant variance (NCV) and has the form (here f is the scalar acceleration at one of the sensors)

$$Y_j = f(t_j, \vec{\theta}_0) + f(t_j, \vec{\theta}_0)\, \epsilon_j \qquad \mathrm{V}(Y_j) = \sigma_0^2\, f^2(t_j, \vec{\theta}_0),$$

and the GLS method is used to estimate $\vec{\theta}_0$, then the distribution of the θ_{GLS} estimator can be approximated as

$$\theta_{\mathrm{GLS}} \sim \mathcal{N}_p(\vec{\theta}_0, \Sigma_0^n) \approx \mathcal{N}_p \left(\vec{\theta}_0, \sigma_0^2 \left(\chi^{nT}(\vec{\theta}_0) W^{-1}(\vec{\theta}_0) \chi^n(\vec{\theta}_0) \right)^{-1} \right), \tag{37}$$

where the sensitivity matrix $\chi(\vec{\theta}) = \chi^n(\vec{\theta}) = \{\chi_{jk}^n\}$ is defined as

$$\chi_{j\,k}^n(\vec{\theta}) = \frac{\partial f(t_j, \vec{\theta})}{\partial \theta_k} \quad j = 1, \ldots, n, \quad k = 1, \ldots, p,$$

and

$$\Sigma_0^n \equiv \sigma_0^2 [n \Omega_0^{\mathrm{GLS}}]^{-1} \tag{38}$$

with

$$\Omega_0^{\mathrm{GLS}} = \lim_{n \to \infty} \frac{1}{n} \chi^{nT}(\vec{\theta}_0) W^{-1}(\vec{\theta}_0) \chi^n(\vec{\theta}_0),$$

(existence of the limit is one of the underlying assumptions of the theory) and $W(\vec{\theta}) = \mathrm{diag}\left(f^2(t_1, \vec{\theta}), \ldots, f^2(t_n, \vec{\theta}) \right)$. Note that since $\vec{\theta}_0$ and σ_0^2 are unknown, the estimates $\hat{\theta} = \hat{\theta}_{\mathrm{GLS}}$, $\hat{\sigma}^2 = \hat{\sigma}^2_{\mathrm{GLS}}$ will be used in (37) to calculate

$$\Sigma_0^n \approx \hat{\Sigma}^n = \hat{\sigma}^2 \left(\chi^{nT}(\hat{\theta}) W^{-1}(\hat{\theta}) \chi^n(\hat{\theta}) \right)^{-1}. \tag{39}$$

The standard errors of the parameters can then be calculated by taking the square root of the diagonal elements of (39). Therefore, in order to obtain the correct standard errors, the correct form of the error generating term and estimation procedure must be specified. That is, if a data set has constant variance *and* the OLS method is used to estimate $\vec{\theta}_0$ then the correct standard error formula is given by (36); similarly, if a data set has nonconstant variance *and* the GLS method is used to estimate $\vec{\theta}_0$ then the correct standard error formula is given by (39). Thus, if the error generating term in the statistical model is not correctly specified any conclusions regarding the standard error are incorrect!!

Although it is imperative that the error structure in the statistical model be specified correctly, we point out that one can also derive asymptotic statistics of an OLS

estimate obtained using NCV generated data. If $\mathrm{Var}(Y_j) = \sigma_0^2 f^2(t_j, \vec{\theta}_0)$ *and* the OLS method is used to estimate $\vec{\theta}_0$ [19], then as $n \to \infty$

$$\theta_{\mathrm{OLS}} \sim \mathcal{N}_p \left(\vec{\theta}_0, \sigma_0^2 \left(\chi^{nT}(\vec{\theta}_0)\chi^n(\vec{\theta}_0) \right)^{-1} \chi^{nT}(\vec{\theta}_0) W(\vec{\theta}_0) \chi^n(\vec{\theta}_0) \left(\chi^{nT}(\vec{\theta}_0)\chi^n(\vec{\theta}_0) \right)^{-1} \right), \quad (40)$$

where $\chi^n(\vec{\theta}_0)$ and $W^{-1}(\vec{\theta}_0)$ have the same definitions as earlier. The underlying conditions necessary for (40) to hold are similar to the conditions mentioned earlier - see [23] for details. Although the OLS procedure is easy to implement and possesses different asymptotic statistics for CV *and* NCV data sets, the OLS estimator is not always the best estimator for a given data set. The reason we assume a data set has constant variance when OLS is employed is because of the asymptotic relative efficiency (ARE) of (39) with respect to (40). The ARE provides a means of determining which estimate converges to its asymptotic variance quicker, and it can be shown that $\hat{\theta}_{\mathrm{GLS}}$ is more efficient than $\hat{\theta}_{\mathrm{OLS}}$ when the data has nonconstant variance [19]. Therefore, we tacitly assume a data set has constant variance when OLS is used to estimate $\vec{\theta}_0$, and would then use (36) to calculate the standard errors of the estimate from the OLS procedure.

A further issue to be resolved is the calculation of the sensitivity matrix $\chi^n(\vec{\theta})$. Because of the complication of the VE wave model, the sensitivity matrix cannot be calculated by analytical techniques and sensitivity equations methods (see [5, 10]) pose significant computational challenges. Instead, we will approximate $\chi^n(\vec{\theta})$ using the first order approximation

$$\chi^n_{jk}(\vec{\theta}) \approx \frac{f(t_j, \vec{\theta} + \vec{h}_k) - f(t_j, \vec{\theta})}{h_k}, \quad (41)$$

where $\vec{h}_k$ is the vector with all components zero except for the scalar h_k in the k^{th} component. However, choosing an appropriate value of h_k is essential to obtaining an accurate approximation. As explained in some detail in [23], one can, with careful but tedious calculations, study the effects of step size h_k on the accuracy in computing standard errors using (41). One can then choose an $\vec{h}_k$ that provides reasonably stable (with respect to $\vec{h}_k$) calculated values of the standard error. Such investigations were used to choose $\vec{h}_k$ in the results presented in Tables 1, 2, 3 and 4.

3.2 Computational Results

We next compare the estimates obtained using the OLS and GLS methods on the CV data set in Tables 1 and 2 and Figure 4. Although one might suspect the OLS estimate to be more accurate than the GLS estimate on the CV data set, it appears the estimates from both methods do equally well in estimating $\vec{\theta}_0$. This observation is bolstered by comparing the graphs of Figure 4 with the top graphs of Figure 3. The main difference between the estimates lies in their respective standard errors. The standard error of the GLS estimate, which is computed using invalid formulas, is much more optimistic than that of the OLS estimate.

Considering the computational results for the CV data set (Tables 1 and 2 and Figure 4), we see that the GLS estimate is as accurate as the OLS estimate. The main difference between the results of the two methods is the corresponding standard error; the standard errors of the GLS estimate are much more appealing than the standard

errors of the OLS estimate. However, the fact that the data has constant variance means that it would be incorrect (indeed meaningless!!) to report the GLS results on this data set, because the expressions for standard errors corresponding to the GLS method are derived under the assumption that the data set has nonconstant variance and hence these expressions have no validity when used with results obtained using CV data.

Table 1: Estimation with OLS procedure and CV data with $\alpha = 3$.

$\vec{\boldsymbol{\theta}}_{\text{init}}$	$\vec{\boldsymbol{\theta}}_{\mathbf{0}}$	$\hat{\boldsymbol{\theta}}^{\text{CV}}_{\text{OLS}}$	**Standard Error**
1100.000	1187.432	1155.660	0.22743310
1400.000	1432.646	1455.667	0.23246094
350.000	386.640	390.278	0.16176841
3400.000	3456.749	3436.025	0.21157166

Table 2: Estimation with GLS procedure and CV data with $\alpha = 3$.

$\vec{\boldsymbol{\theta}}_{\text{init}}$	$\vec{\boldsymbol{\theta}}_{\mathbf{0}}$	$\hat{\boldsymbol{\theta}}^{\text{CV}}_{\text{GLS}}$	**Standard Error**
1100.000	1187.432	1162.446	0.04007688
1400.000	1432.646	1462.446	0.04062001
350.000	386.640	384.670	0.03158570
3400.000	3456.749	3446.752	0.03797396

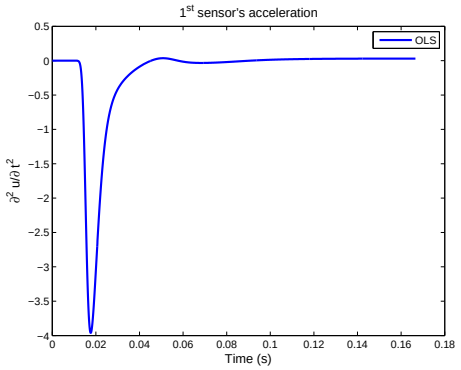

Plot of model response corresponding to $\hat{\theta}^{\text{CV}}_{\text{OLS}}$

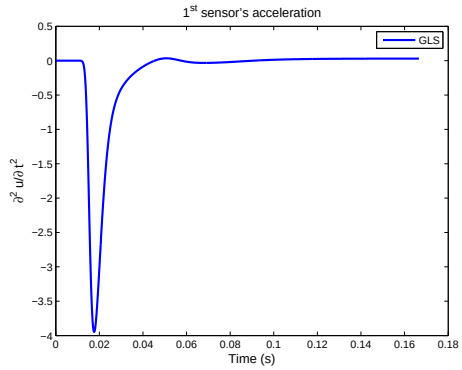

Plot of model response corresponding to $\hat{\theta}^{\text{CV}}_{\text{GLS}}$

Figure 4: Comparison of estimates with CV data for 1st sensor with $\alpha = 3$.

We also compared the estimates obtained using the OLS and GLS methods on the NCV data set (Tables 3 and 4 and Figure 5). Although one might suspect the GLS estimate to be more accurate than the OLS estimate on the nonconstant variance data set it (again) appears the estimates from both methods do equally well in estimating $\vec{\theta}_0$. This observation is again bolstered by comparing the graphs in Figure 5 with the top graphs of Figure 3. The main difference between the estimates (again) lies in their respective standard errors. The standard errors of the GLS estimate are still more

Table 3: Estimation with OLS procedure NCV data with $\alpha = 3$.

$\vec{\boldsymbol{\theta}}_{\text{init}}$	$\vec{\boldsymbol{\theta}}_{\mathbf{0}}$	$\hat{\boldsymbol{\theta}}^{\text{NCV}}_{\text{OLS}}$	**Standard Error**
1100.000	1187.432	1161.867	0.07329180
1400.000	1432.646	1461.869	0.07170462
350.000	386.640	384.895	0.05162474
3400.000	3456.749	3474.578	0.07734921

Table 4: Estimation with GLS procedure and NCV data with $\alpha = 3$.

$\vec{\boldsymbol{\theta}}_{\text{init}}$	$\vec{\boldsymbol{\theta}}_{\mathbf{0}}$	$\hat{\boldsymbol{\theta}}^{\text{NCV}}_{\text{GLS}}$	**Standard Error**
1100.000	1187.432	1163.501	0.01863883
1400.000	1432.646	1463.501	0.01899244
350.000	386.640	386.557	0.01474706
3400.000	3456.749	3448.968	0.01774607

Table 5: Standard errors obtained with different estimates $\hat{\theta}$ ($\alpha = 3$).

$\text{SE}(\hat{\boldsymbol{\theta}}^{\text{CV}}_{\text{OLS}})$	$\text{SE}(\hat{\boldsymbol{\theta}}^{\text{NCV}}_{\text{OLS}})$	$\text{SE}(\hat{\boldsymbol{\theta}}^{\text{CV}}_{\text{GLS}})$	$\text{SE}(\hat{\boldsymbol{\theta}}^{\text{NCV}}_{\text{GLS}})$
.2356770	.2618172	.2682730	.0121120
.2267969	.2700248	.2686650	.0119206
.1619844	.8086739	.1594453	.0120431
.2336860	.5258509	.2627922	.0124671

optimistic than that of the OLS estimate, but now the GLS results are correct since the data set has nonconstant variance. Use of the OLS based standard errors would give incorrect estimates for the uncertainty in parameter estimates.

An interesting observation from the simulations reported in Tables 1 - 4 is that the standard errors for the GLS estimate are more optimistic than that of the OLS estimate. Before one makes any generalizations regarding which estimates have more optimistic standard errors, recall that the estimates $\hat{\theta}_{\text{OLS}}$ and $\hat{\theta}_{\text{GLS}}$ are realizations of the random variables θ_{OLS} and θ_{GLS}, and also that the standard errors depend upon the value of the estimate $\hat{\theta}_{\text{OLS}}$ and $\hat{\theta}_{\text{GLS}}$. Hence, two realizations of θ_{OLS} (or θ_{GLS}) will in general produce two different estimates $\hat{\theta}_{\text{OLS}}$ ($\hat{\theta}_{\text{GLS}}$), which in turn will generate two different standard errors. For instance, Table 5 displays standard errors for estimates obtained from different realizations $\{y_j\}$ of the observation process $\{Y_j\}$ than that of Tables 1 - 4. As expected, the standard errors for the estimates are different than those from the first simulation. What is most striking, however, is that the GLS estimate is no longer always more optimistic than the OLS estimate. Thus, when possible, conclusions regarding the accuracy of an estimator should be based on a large number of realizations (i.e., multiple longitudinal data sets if available) of that estimator - a process that is described in detail in [23]. Nonetheless, the computations with simulated CV and NCV "data" sets discussed in this section suggest the feasibility of accurate estimation of material parameters in models such as (1)-(6) with data containing either absolute or relative error as long as the correct inverse problem formulations are employed.

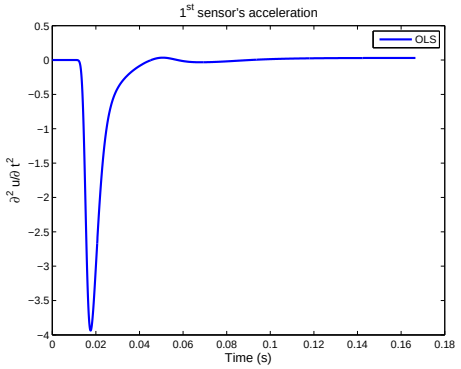

Plot of model response corresponding to $\hat{\theta}^{\text{NCV}}_{\text{OLS}}$

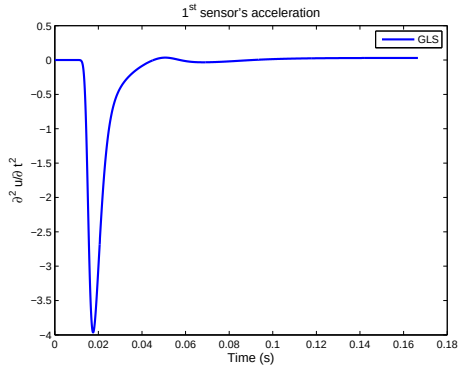

Plot of model response corresponding to $\hat{\theta}^{\text{NCV}}_{\text{GLS}}$

Figure 5: Comparison for estimates with NCV data for 1st sensor with $\alpha = 3$.

4 Estimating Occlusion Parameters q_1 and q_2

Now that we have demonstrated the effectiveness of the OLS and GLS estimators in estimating the parameters C_{λ_k} and C_{μ_k} with noisy data, we turn our attention to estimating the geometric occlusion parameters q_1 and q_2. We initially deferred estimating q_1 and q_2 because the model is discontinuous with respect to these parameters if formulated directly based on the discontinuous geometry of Figure 2; this makes the estimation procedure somewhat challenging. In fact, previous efforts [21] encountered difficulties estimating the occlusion geometric parameters even when there was no noise introduced into the measurement data. A sampling of the results from that work is summarized in Table 6 where Matlab's *fminsearch* was used to minimize the OLS estimating equation (28). Difficulties arose even though *fminsearch* is a direct search method not requiring derivatives. Of particular concern are cases where the optimization routine simply returns the initial guess, such as when $q_0 = [\pi/6, 5\pi/6] = [.523598, 2.617993]$.

Table 6: OLS estimation in 2D *dis*continuous model and data with no noise.

initial parameters	optimal parameters	true parameters	relative error
$\frac{\pi}{4}$= .785398	.790306	.785398	0.6%
$\frac{3\pi}{4}$= 2.356194	2.422462	2.356194	2.81%
$\frac{\pi}{3}$= 1.047197	.929387	.785398	18.3%
$\frac{2\pi}{3}$=2.094395	2.336559	2.356194	.833%
$\frac{\pi}{6}$= .523598	.523598	.785398	33.3%
$\frac{5\pi}{6}$=2.617993	2.617933	2.356194	11.1%
$\frac{\pi}{2}$= 1.570796	.711527	.785398	9.4%
$\frac{\pi}{2}$= 1.570796	2.36885	2.356194	.53%

To attempt to obtain better results we reformulated the model in terms of a smoother (continuous) geometry with respect to q_1 and q_2 and utilized the *iteratively re-weighted least squares* (IRWLS) algorithm for GLS estimators. IRWLS is an iterative approach to calculating the GLS estimate, but instead of solving the defining

normal equations for GLS estimators (see [5, 15]), one iteratively solves

$$\theta_{\text{GLS}}^{(k+1)} = \arg\min_{\vec{\theta}\in\Theta} \sum_{j=1}^{n} w_j^{(k)} \left(Y_j - f\big(t_j, \vec{\theta}\big) \right)^2, \tag{42}$$

where $w_j^{(k)} = f^{-2}(t_j, \theta_{\text{GLS}}^{(k)})$ [5, 15]. In addition to providing a potential improvement in parameter estimation, one could argue that a continuous occlusion geometry is closer to the physical characteristics of a arterial stenosis. To implement the continuous occlusion geometry, the signal from the input will be impeded, at a linear rate, near q_1 and q_2 (see Figure 6). That is, the impulse function along the arterial wall will be defined as $f_{11}(t, \phi, z) = r(\phi) w_1(t, R_1, \phi, z)$, where

$$r(\phi) = \begin{cases} 0, & \phi \in (q_1, q_2) \\ \frac{1}{\delta}(q_1 - \phi), & \phi \in (q_1 - \delta, q_1) \\ \frac{1}{\delta}(\phi - q_2), & \phi \in (q_2, q_2 + \delta) \\ 1, & \text{otherwise} \end{cases} \tag{43}$$

denotes the ramp function and δ indicates the distance from q_1 and q_2 at which the impulse function is no longer occluded. Matlab's *fminsearch* was used in both the OLS and GLS estimating procedures. Gradient-based, trust region optimization methods, such as *lsqnonlin*, were attempted, but the errors in the estimates were significant while the computation time remained about the same as that found using *fminsearch*.

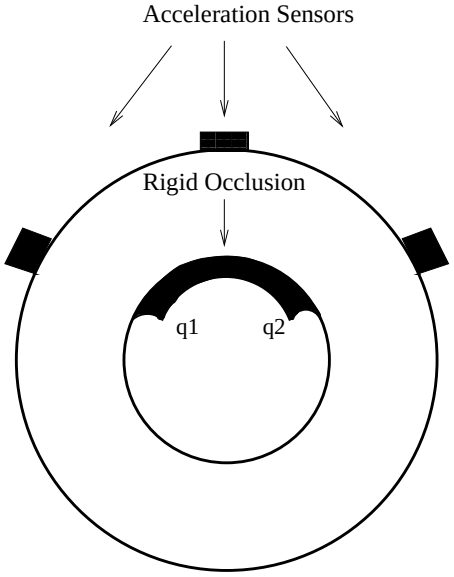

Figure 6: Altered occlusion allows model to depend continuously on q_1, q_2.

The OLS and GLS results obtained from using *fminsearch* (with the continuous model) are given in Tables 7 and 8 respectively. These results are an improvement from the estimates obtained for the *dis*continuous model with *fminsearch*. In particular, when the exact solution is the initial value in the optimization routine, we expect the routine to return the exact solution when the forward-generated data has no noise. That didn't happen with the discontinuous model, but does occur with the

continuous model. Another encouraging finding when we used the continuous model with *fminsearch* is that the optimal value is not the same as the initial value for any of the optimizations. This situation arose with the discontinuous model (see the third simulation in Table 6) and is one of the more troubling aspects of the discontinuous model. When the continuous model is optimized using *fminsearch* (Tables 7 and 8), the estimates for both q_1 and q_2 for *all* the inverse problem results using data generated with no noise are excellent. To permit ready comparison with the results of [21] and Table 6, we list in Tables 7 and 8 the relative error in the estimate as compared to the true parameter value. Thus, we will use the continuous model with the *fminsearch*

Table 7: OLS estimation results, 2D continuous model, no noise data.

initial parameters	optimal parameters	$\vec{\theta}_0$	relative error
$\frac{\pi}{4}$= .785398	.78540	.78540	0%
$\frac{3\pi}{4}$= 2.356194	2.3562	2.3562	0%
$\frac{\pi}{3}$= 1.047197	.78536	.78540	.00510%
$\frac{2\pi}{3}$=2.094395	2.3562	2.3562	0%
$\frac{\pi}{6}$= .523598	.78540	.78540	0%
$\frac{5\pi}{6}$= 2.617993	2.3562	2.3562	0%
$\frac{\pi}{2}$= 1.570796	.78538	.78540	.00255%
$\frac{\pi}{2}$= 1.570796	2.3562	2.3562	0%

Table 8: GLS estimation results, 2D continuous model, no noise data.

initial parameters	optimal parameters	$\vec{\theta}_0$	relative error
$\frac{\pi}{4}$= .785398	.78540	.78540	0%
$\frac{3\pi}{4}$= 2.356194	2.3562	2.3562	0%
$\frac{\pi}{3}$= 1.047197	.78540	.78540	0%
$\frac{2\pi}{3}$=2.094395	2.3562	2.3562	0%
$\frac{\pi}{6}$= .523598	.78540	.78540	0%
$\frac{5\pi}{6}$= 2.617993	2.3562	2.3562	0%
$\frac{\pi}{2}$= 1.570796	.78540	.78540	0%
$\frac{\pi}{2}$= 1.570796	2.3562	2.3562	0%

optimization routine to approximate the location of the occlusion when the data has been corrupted by noise varying between 2% and 10%. We also used initial estimates $q_1 = q_2$ in $\vec{\theta}_{\text{init}}$ in obtaining the results presented in Tables 9, 10, 11 and 12. This initialization is equivalent to assuming no blockages are present in the artery.

Table 9: OLS estimation in 2D continuous model with CV error.

$\boldsymbol{\alpha}$	initial parameters	optimal parameters	$\vec{\theta}_0$	relative error	SE
2	$\frac{\pi}{2}$=1.570796	.78539	.78540	0%	2.3728e-05
	$\frac{\pi}{2}$=1.570796	2.3562	2.3562	0%	1.8217e-05
4	$\frac{\pi}{2}$=1.570796	.78539	.78540	.00127%	5.0233e-05
	$\frac{\pi}{2}$=1.570796	2.3562	2.3562	0%	3.7085e-05
8	$\frac{\pi}{2}$=1.570796	.78555	.78540	.0191%	9.8035e-05
	$\frac{\pi}{2}$=1.570796	2.3562	2.3562	0%	7.1959e-05
10	$\frac{\pi}{2}$=1.570796	.78534	.78540	.00764%	1.2347e-04
	$\frac{\pi}{2}$=1.570796	2.3562	2.3562	0%	9.0529e-05

Table 10: OLS estimation in 2D continuous model with NCV error.

$\boldsymbol{\alpha}$	initial parameters	optimal parameters	$\vec{\theta}_0$	relative error	SE
2	$\frac{\pi}{2}$=1.570796	.78541	.78540	.00127%	3.7059e-04
	$\frac{\pi}{2}$=1.570796	2.3562	2.3562	0%	3.6991e-04
4	$\frac{\pi}{2}$=1.570796	.78490	.78540	.0637%	7.3616e-04
	$\frac{\pi}{2}$=1.570796	2.3557	2.3562	.0212%	7.4441e-04
8	$\frac{\pi}{2}$=1.570796	.78501	.78540	.0450%	1.5360e-03
	$\frac{\pi}{2}$=1.570796	2.3560	2.3562	.00849%	1.5454e-03
10	$\frac{\pi}{2}$=1.570796	.78435	.78540	.13%	1.8835e-03
	$\frac{\pi}{2}$=1.570796	2.3569	2.3562	.0297%	1.8889e-03

The time it took to compute estimates for q_1 and q_2 was between 800 - 900 seconds and 1000 - 2500 seconds, respectively, for the OLS and GLS methods using *fminsearch* We also carried out these same computations using *lsqnonlin* and the time it took to compute q_1 and q_2 in this case was between 800 - 900 seconds each for the OLS and GLS methods .

Just as in the previous section, one needs to address the approximation of the sensitivity matrix χ^n. Again, a forward difference scheme was used to approximate χ^n, and an appropriate step size $\vec{h}$ was determined; details can be found in [23]. The results in Tables 9 and 12 suggest that even in the presence of 10% noise in either the CV or NCV data cases, one can readily estimate the geometric occlusion parameters with reasonable accuracy.

On the other hand, comparison of Tables 9 and 10 and Tables 11 and 12 suggest that one cannot, in general, determine whether the correct statistical model (and corresponding correct method OLS or GLS) has been assumed by simply looking at the estimates obtained or comparing the standard errors when the true parameter values are not known. Thus, in dealing with experimental data and unknown parameters in a model, one needs post analysis techniques to ascertain whether the correct statistical model and correct asymptotic expressions for the standard error have been assumed. This will be the focus of our discussions on residual plots.

Table 11: GLS estimation in 2D continuous model with CV error.

$\boldsymbol{\alpha}$	initial parameters	optimal parameters	$\vec{\theta}_0$	relative error	SE
2	$\frac{\pi}{2}$=1.570796	.786541	.78540	.15%	2.055343e-04
	$\frac{\pi}{2}$=1.570796	2.353690	2.3562	.11%	2.054282e-04
4	$\frac{\pi}{2}$=1.570796	.784193	.78540	.15%	3.899241e-04
	$\frac{\pi}{2}$=1.570796	2.356844	2.3562	.028%	3.897943e-04
8	$\frac{\pi}{2}$=1.570796	.785371	.78540	.0035%	7.816567e-04
	$\frac{\pi}{2}$=1.570796	2.356133	2.3562	.0026%	7.813815e-04
10	$\frac{\pi}{2}$=1.570796	.785114	.78540	.036%	9.719429e-04
	$\frac{\pi}{2}$=1.570796	2.356181	2.3562	.00058%	9.715764e-04

Table 12: GLS estimation in 2D continuous model with NCV error.

$\boldsymbol{\alpha}$	initial parameters	optimal parameters	$\vec{\theta}_0$	relative error	SE
2	$\frac{\pi}{2}$=1.570796	.785422	.78540	.0031%	2.071356e-02
	$\frac{\pi}{2}$=1.570796	2.356179	2.3562	.00064%	2.073407e-02
4	$\frac{\pi}{2}$=1.570796	.785401	.78540	.00033%	4.038974e-02
	$\frac{\pi}{2}$=1.570796	2.356166	2.3562	.0012%	4.041175e-02
8	$\frac{\pi}{2}$=1.570796	.785321	.78540	.0099%	8.153026e-02
	$\frac{\pi}{2}$=1.570796	2.356328	2.3562	.0057%	8.157475e-02
10	$\frac{\pi}{2}$=1.570796	.785165	.78540	.03%	1.025934e-01
	$\frac{\pi}{2}$=1.570796	2.356243	2.3562	.0021%	1.024360e-01

5 Residual Plots

One can carry out simulation studies with a proposed mathematical model to assist in understanding the behavior of the model in inverse problems with different types of data with respect to mis-specification of the statistical model. For example, we consider a statistical model with constant variance noise

$$Y_j = f(t_j, \vec{\theta}_0) + \frac{\alpha}{100}\epsilon_j, \qquad \mathrm{Var}(Y_j) = \frac{\alpha^2}{10000}\sigma_0^2,$$

and nonconstant variance noise

$$Y_j = f(t_j, \vec{\theta}_0)\left(1 + \frac{\alpha}{100}\epsilon_j\right), \qquad \mathrm{Var}(Y_j) = \frac{\alpha^2}{10000}\sigma_0^2\, f^2(t_j, \vec{\theta}_0).$$

We can obtain a data set by considering a *realization* $\{y_j\}_{j=1}^n$ of the random process $\{Y_j\}_{j=1}^n$ through a realization of $\{\epsilon_j\}_{j=1}^n$ and then calculate an estimate $\hat{\theta}$ of $\vec{\theta}_0$ using the OLS or GLS procedure. Here $f = f_i$ is the model response (i.e., acceleration $\frac{\partial^2 u_1}{\partial t^2}$) at one of the sensors.

We can then use the residuals $r_j = y_j - f(t_j, \hat{\theta})$ to test whether the data set is *i.i.d.* and possesses the assumed variance structure. If a data set has constant variance error then

$$Y_j = f(t_j, \vec{\theta}_0) + \epsilon_j \quad \text{or} \quad \epsilon_j = Y_j - f(t_j, \vec{\theta}_0).$$

Because it is assumed that the error ϵ_j is *i.i.d.*, a plot of the residuals $r_j = y_j - f(t_j, \hat{\theta})$ vs. t_j should be random. Also, the error in the constant variance case does not depend on $f(t_j, \theta_0)$, and so a plot of the residuals $r_j = y_j - f(t_j, \hat{\theta})$ vs. $f(t_j, \hat{\theta})$ should also be random. Therefore, *if* the error has constant variance then plots of the residuals $r_j = y_j - f(t_j, \hat{\theta})$ against t_j and against $f(t_j, \hat{\theta})$ should both be random. If not, then the independent constant variance assumption is suspect.

We turn next to questions of what to expect if this residual test is applied to a data set that has nonconstant variance generated error. That is, we wish to investigate what happens if the data are incorrectly assumed to have constant variance error when in fact they have nonconstant variance error. Because in the nonconstant variance example, $R_j = Y_j - f(t_j, \vec{\theta}_0) = f(t_j, \vec{\theta}_0)\,\epsilon_j$ depends upon the deterministic model $f(t_j, \vec{\theta}_0)$, we should expect that a plot of the residuals $r_j = y_j - f(t_j, \hat{\theta})$ vs. t_j should exhibit some type of pattern. Also, the residuals actually depend on $f(t_j, \hat{\theta})$ in the nonconstant variance case, and so as $f(t_j, \hat{\theta})$ increases the variation of the residuals $r_j = y_j - f(t_j, \hat{\theta})$ should increase as well. Thus $r_j = y_j - f(t_j, \hat{\theta})$ vs. $f(t_j, \hat{\theta})$ should have a fan shape in the nonconstant variance case.

In summary, if a data set has nonconstant variance generated data, then

$$Y_j = f(t_j, \vec{\theta}_0) + f(t_j, \vec{\theta}_0)\,\epsilon_j \quad \text{or} \quad \epsilon_j = \frac{Y_j - f(t_j, \vec{\theta}_0)}{f(t_j, \vec{\theta}_0)}.$$

If the distribution ϵ_j is *i.i.d.*, then a plot of the *modified residuals* $r_j^m = (y_j - f(t_j, \hat{\theta}))/f(t_j, \hat{\theta})$ vs. t_j should be random for nonconstant variance generated data. A plot of $r_j^m = (y_j - f(t_j, \hat{\theta}))/f(t_j, \hat{\theta})$ vs. $f(t_j, \hat{\theta})$ should also be random.

Another question of interest concerns the case in which the data are incorrectly assumed to have nonconstant variance error when in fact they have constant variance

error. Because $Y_j - f(t_j, \vec{\theta}_0) = \epsilon_j$ in the constant variance case, we should expect that a plot of $r_j^m = (y_j - f(t_j, \hat{\theta}))/f(t_j, \hat{\theta})$ vs. t_j as well as that for $r_j^m = (y_j - f(t_j, \hat{\theta}))/f(t_j, \hat{\theta})$ vs. $f(t_j, \hat{\theta})$ will possess some distinct pattern.

There are further issues regarding residual plots: As we shall see by examples, some data sets might have values that are repeated or nearly repeated a large number of times (for example when sampling near an equilibrium for the mathematical model or when sampling a periodic system over many periods). If a certain value is repeated numerous times (e.g., f_{repeat}) then any plot with $f(t_j, \hat{\theta})$ along the horizontal axis should have a cluster of values along the vertical line $x = f_{\text{repeat}}$. This feature can easily be removed by excluding the data points corresponding to these high frequency values (or simply excluding the corresponding points in the residual plots). Another common technique when plotting against model predictions is to plot against $log\ f(t_j, \hat{\theta})$ instead of $f(t_j, \hat{\theta})$ itself which has the effect of "stretching out" plots at the ends. Also, note that the model value $f(t_j, \hat{\theta})$ could possibly be zero or very near zero, in which case the modified residuals $r_j^m = \frac{y_j - f(t_j, \hat{\theta})}{f(t_j, \hat{\theta})}$ would be undefined or extremely large. To remedy this situation one might exclude values very close to zero (in either the plots or in the data themselves). We chose here to reduce the data sets (although this sometimes could lead to a deterioration in the estimation results obtained). In our examples below, estimates obtained using a truncated data set will be denoted by $\hat{\theta}_{\text{OLS}}^{\text{tCV}}$ for constant variance data and $\hat{\theta}_{\text{OLS}}^{\text{tNCV}}$ for nonconstant variance data.

6 VE Wave Model Residual Plots

The residual tests described in Section 5 will be applied to the VE wave propagation model. The setup for the tests is exactly the same as was described earlier - the OLS and GLS methods will be used to estimate $\vec{\theta}_0$ on data sets with constant and nonconstant variance noise. In order to avoid dense vertical lines (occurring when one has many repeated model values in the plots) and division by zero (when model values are nearly zero), we consider the truncated data sets. Inspecting Figure 7 we see that there are high frequency repeated values near $f(t_j, \vec{\theta}_0) = 0$ and $f(t_j, \vec{\theta}_0) = -.02$ for the 8^{th} sensor; thus the truncated data set will not include model values that are near zero or $-.02$ (which simultaneously alleviates problems of dividing by zero when computing modified residuals). Using truncated data plots (compare Figures 8 and 9; one draws the same conclusions from either plot) makes analysis somewhat easier (patterns are easier to discern) in many cases. More importantly, though, when using the truncated data set, the modified residuals no longer blowup, and this makes the conclusions regarding the error structure straightforward. Thus, for our presentation here, we investigate residual plots with truncated data sets (corresponding residuals computed from full data sets can be found [23]) for two different statistical models:

$$\vec{Y}_j = \vec{f}(t_j, \vec{\theta}_0) + \alpha \vec{\epsilon}_j \qquad \vec{\epsilon}_j^{\,i} \sim \max_k \left| f_i(t_k, \vec{\theta}_0) \right| \mathcal{N}(0, 1), \tag{44}$$

$$Y_j = f(t_j, \vec{\theta}_0)\,(1 + \alpha \epsilon_j) \qquad \epsilon_j \sim \mathcal{N}(0, 1). \tag{45}$$

As we mentioned earlier, both methods (OLS and GLS) do a reasonable job at estimating $\vec{\theta}_0$ in the VE wave propagation model; however the error structure was

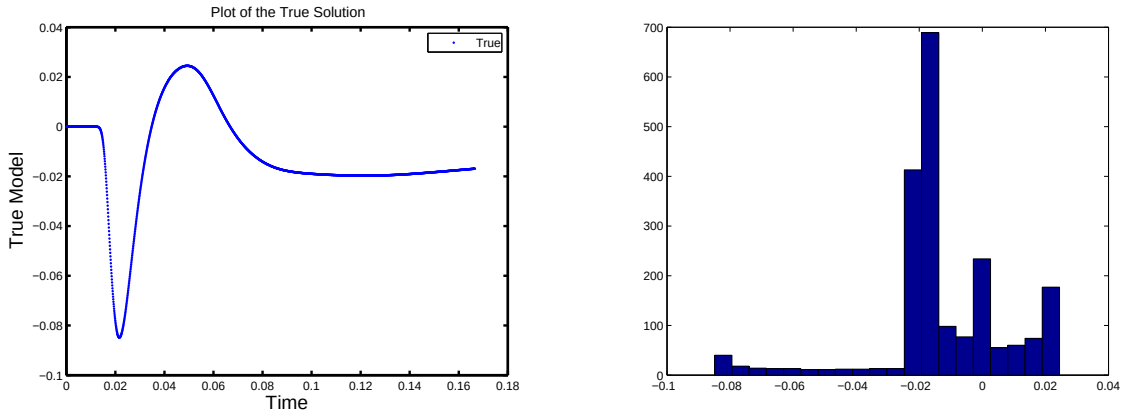

Figure 7: 8^{th} sensor output, and corresponding histogram (model values no noise).

not always correctly specified. That is, the OLS method was applied to nonconstant variance data and the GLS method was applied to constant variance data. We expect the residual plots to reveal these statistical model choice mistakes. The plot of the residuals for $\hat{\theta}^{\text{NCV}}_{\text{OLS}}$ given in Figure 10 reveals a fan shaped pattern, which indicates the constant variance assumption is suspect. In addition, the plot of the residuals for $\hat{\theta}^{\text{CV}}_{\text{GLS}}$ given in Figure 11 reveals the residuals have a deterministic structure, which indicates the nonconstant variance assumption is suspect. As expected, when the correct error structure is assumed, the *i.i.d.* test and the model dependence test both display a random pattern (Figures 9 and 12).

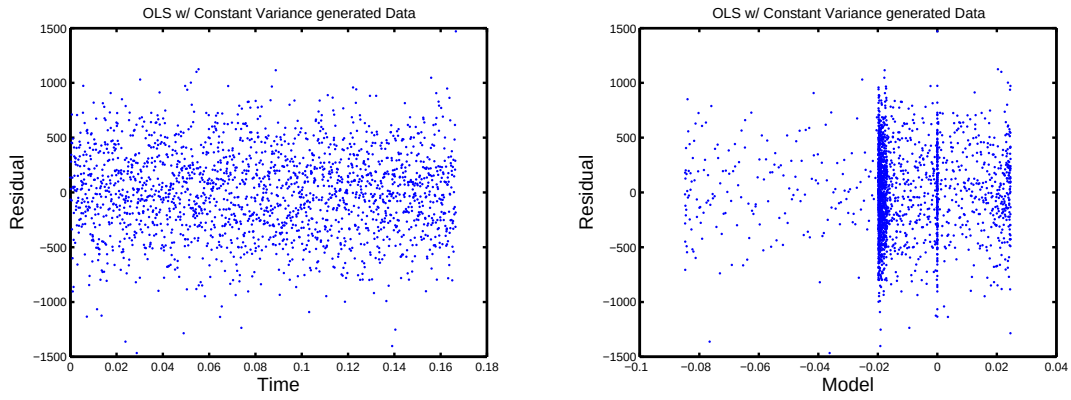

Figure 8: 8^{th} sensor's residual plots for $\hat{\theta}^{\text{CV}}_{\text{OLS}}$ with $\alpha = 3$.

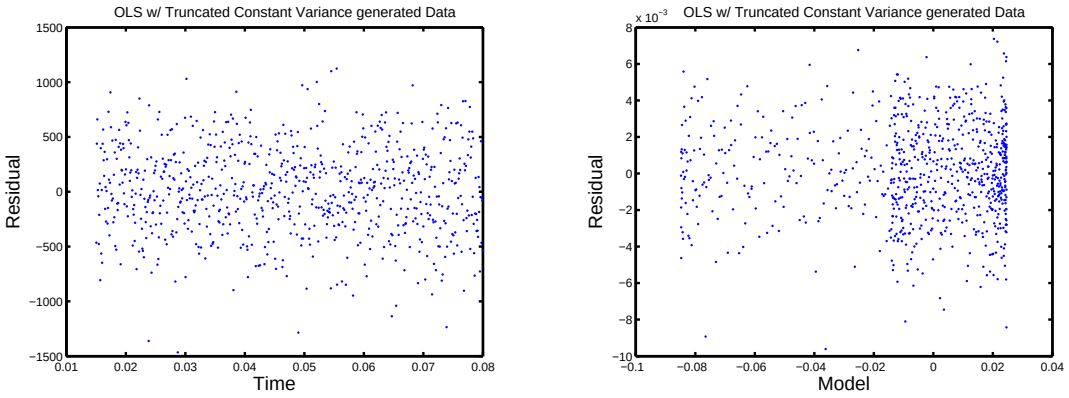

Figure 9: 8^{th} sensor's residual plots for $\hat{\theta}_{\text{OLS}}^{\text{tCV}}$ with $\alpha = 3$.

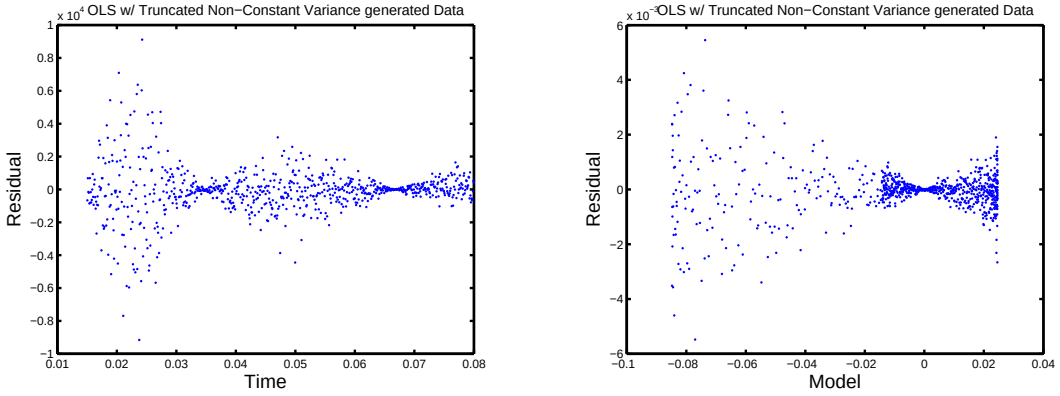

Figure 10: 8^{th} sensor's residual plots for $\hat{\theta}_{\text{OLS}}^{\text{tNCV}}$ with $\alpha = 3$.

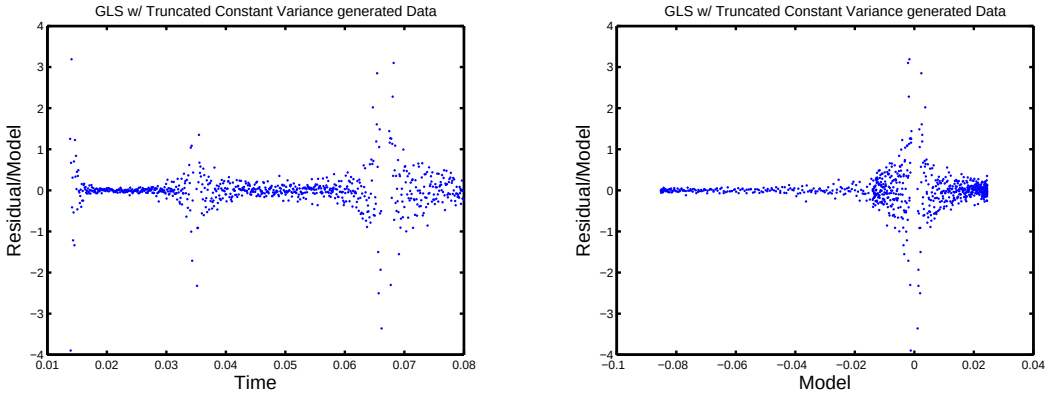

Figure 11: 8^{th} sensor's residual plots for $\hat{\theta}_{\text{GLS}}^{\text{tCV}}$ with $\alpha = 3$.

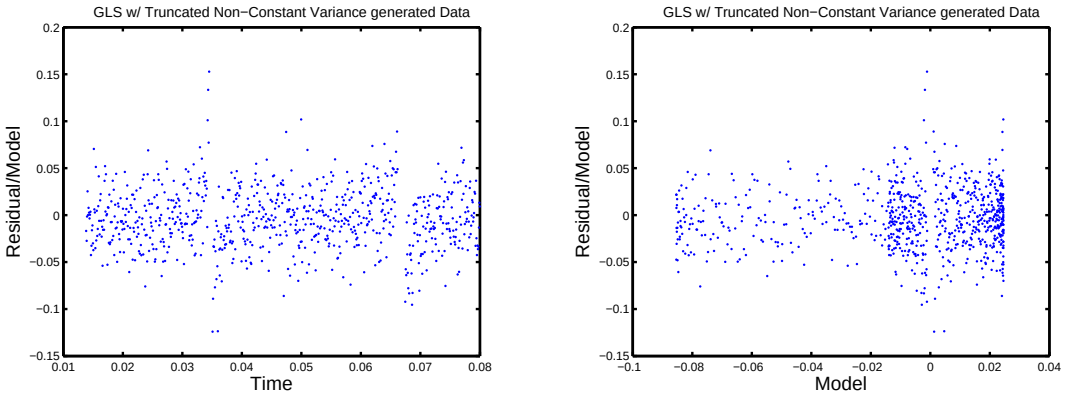

Figure 12: 8^{th} sensor's residual plots for $\hat{\theta}_{\text{GLS}}^{\text{tNCV}}$ with $\alpha = 3$.

7 Concluding Remarks

In the presentation here we have attempted to demonstrate the effectiveness of inverse problem methodology in identifying both material and geometric occlusion parameters such as C_{λ_k}, q_1 and q_2 in a 2D model for arterial stenosis detection using viscoelastic wave propagation. A major concern as one prepares experiments for validation of the stenosis detection concept is the performance of inverse problem methodology for use with actual experimental data. By establishing that the inverse problem can be used to accurately detect and identify the geometric occlusion parameters q_1 and q_2 with simulated data, we have shown that the ISV is not only a possible viable description of VE wave propagation and deserves to be tested against experimental data, but that the related inverse problem techniques could be readily developed in possible stenosis detection procedures for use by the medical community. A significant component of the contribution here explores various statistical techniques that can be used to assess the underlying model assumptions of an experimental data set. After presenting various statistical methods to achieve that goal, we tested those methods on the ISV model with simulated data. The results support our expectations that the proposed inverse problem methodology can be effectively used in carefully chosen mathematical and statistical representations for acceleration data in stenosis detection.

There are other techniques that one could use to further investigate inverse problems in elasticity/viscoelasticity wave propagation. Among these are:

- Monte Carlo simulations are useful to help determine typical results from asymptotic statistical theory. In particular, MC simulations with multiple simulated data sets can be used to investigate the accuracy of asymptotic based standard errors and confidence intervals for a given problem with respect sample size as well as other factors such as number of iterations used in GLS IRWLS algorithms (see [23] for example calculations).
- Pre-experiment inverse problem calculations can be carried out to provide information on properties (sample size, sampling frequency, duration of experiments, etc.) of data sets needed to identify specific parameters as was done for example in design of experiments with shrimp to support and validate complex growth rate dynamic models-see [6].
- Finally, one can also use traditional sensitivity functions (TSF) and generalized sensitivity functions (GSF) to investigate which parameters are mostly likely to accurately be identified with what types (how much, how often and when to sample, etc.) of data for a given class of models-see [7, 8, 9, 10, 14, 25].

Acknowledgements

This research was supported in part by the U.S. Air Force Office of Scientific Research under grant AFOSR-FA9550-08-1-0147 and in part by the National Institute of Allergy and Infectious Disease under grant NIAID 9R01AI071915-05.

References

[1] E. Awtry and J. Loscalzo, Coronary heart disease, *Cecil Essentials of Medicine*, **6** (2004), 87–108.

[2] H.T. Banks, J.H. Barnes, A. Eberhardt, H. Tran, and S. Wynne, Modeling and computation of propagating waves from coronary stenoses, *Computation and Applied Mathematics*, **21** (2002), 767–788.

[3] H.T. Banks and K.L. Bihari, Modeling and estimating uncertainty in parameter estimation, *Inverse Problems*, **17** (2001), 95–111.

[4] H.T. Banks, D.M. Bortz, G.A. Pinter and L.K. Potter, Modeling and imaging techniques with potential for application in bioterrorism, Chapter 6 in *Bioterrorism: Mathematical Modeling Applications in Homeland Security*, (H.T. Banks and C. Castillo-Chavez, eds.), Frontiers in Applied Mathematics **FR28**, SIAM, Philadelphia, 2003, pp. 129–154.

[5] H.T. Banks, M. Davidian, J. Samuels and K. Sutton, An inverse problem statistical methodology summary, *CRSC Tech Report*, CRSC-TR08-01, NCSU, January, 2008; in *Statistical Estimation Approaches in Epidemiology*, (edited by Gerardo Chowell, Mac Hyman, Nick Hengartner, Luis M.A Bettencourt and Carlos Castillo-Chavez), Springer, Berlin Heidelberg New York, to appear.

[6] H.T. Banks, J.L. Davis, S.L. Ernstberger, S. Hu, E. Artimovich, and A.K. Dhar, Experimental design and estimation of growth rate distributions in size-structured shrimp populations, *CRSC Tech Report*, CRSC-TR08-20, NCSU, November, 2008.

[7] H.T. Banks, S. Dediu and S.E. Ernstberger, Sensitivity functions and their uses in inverse problems, *CRSC Tech Report*, CRSC-TR07-12, NCSU, July, 2007; *J. Inverse and Ill-posed Problems*, **15** (2007), 683–708.

[8] H.T. Banks, Sava Dediu, Stacey L. Ernstberger and Franz Kappel, A new approach to optimal design problems, *CRSC Tech Report*, CRSC-TR08-12, NCSU, September, 2008.

[9] H. T. Banks, S. Dediu and H. K. Nguyen, Sensitivity of dynamical systems to parameters in a convex subset of a topological vector space, *Math. Biosci. and Engineering*, **4** (2007), 403–430.

[10] H.T. Banks, S. Ernstberger, and S. Grove. Standard errors and confidence intervals in inverse problems: sensititivty and associated pitfalls, *CRSC Tech Report*, CRSC-TR06-10, March, 2006; *J. Inverse and Ill-posed Problems*, **15** (2007), 1–18.

[11] H.T. Banks and N. Luke, Modelling of propagating shear waves in biotissue employing an internal variable approach to dissipation. *Communication in Computational Physics*, **3** (2008), 603–640.

[12] H.T. Banks, N. Medhin, and G. Pinter, Multiscale considerations in modeling of nonlinear elastomers, *International Journal for Computational Methods in Engineering Science and Mechanics*, **8** (2007), 53–62.

[13] H.T. Banks and G.A. Pinter, A probabilistic multiscale approach to hysteresis in shear wave propagation in biotissue, CRSC-TR04-03, NCSU, January, 2004; *SIAM J. Multiscale Modeling and Simulation,* **2** (2005), 395–412.

[14] J. J. Batzel, F. Kappel, D. Schneditz and H. T. Tran, *Cardiovascular and Respiratory Systems: Modeling, Analysis and Control*, SIAM Frontiers in Applied Math, SIAM, Philadelphia, 2006.

[15] M. Davidian and D. Giltinan, *Nonlinear Models for Repeated Measurement Data*, Chapman & Hall, London, 1998.

[16] M. Delgado, Semiparametric generalized least squares in the multivariate nonlinear regression model, *Econometric Theory*, **8** (1992), 203–222.

[17] Y. Fung, *Biomechanics: Mechanical Properties of Living Tissues*, Spring-Verlag, New York, 1993.

[18] Y. Fung, *A First Course in Continuum Mechanics*, Prentice Hall, Englewood Cliffs, NJ, 1994.

[19] M. Gumpertz and S. Pantula, Nonlinear regression with variance components, *Journal of the American Statistical Association*, **87** (1992), 201–209.

[20] A.E.H. Love, *Mathematical Theory of Elasticity*, Cambridge University Press, London, 1927.

[21] N. Luke, Modeling shear wave propagation in biotissue: An internal variable approach to dissipation, Ph.D. thesis, North Carolina State University, Raleigh, NC http://www.ncsu.edu/grad/etd/online.html, 2006.

[22] W. Rosamond et al., Heart disease and stroke statistics-2007 update: A report from the American Heart Association statistics committee and Stroke Statistics Subcommittee, *Circulation*, **115** (2007).

[23] J. Samuels, Inverse Problems and Post Analysis Techniques for a Stenosis-Driven Acoustic Wave Propagation Model, Ph.D. thesis, North Carolina State University, Raleigh, NC, http://www.ncsu.edu/grad/etd/online.html,2008.

[24] G. Seber and J. Wild, *Nonlinear Regression*, Wiley, New York, 2003.

[25] K. Thomaseth and C. Cobelli, Generalized sensitivity functions in physiological system identification, *Annals of Biomedical Engineering*, **27** (1999), 607–616.